Rapid Uptake of Gold Nanorods by Primary Human Blood Phagocytes and Immunomodulatory Effects of Surface Chemistry

Matthias Bartneck,[†,¶,*] Heidrun A. Keul,[‡,¶] Smriti Singh,[‡] Katharina Czaja,[§] Jörg Bornemann,[⊥] Michael Bockstaller,[∥] Martin Moeller,[‡] Gabriele Zwadlo-Klarwasser,[†,§] and Jürgen Groll[‡,*]

[†]Interdisciplinary Centre for Clinical Research BioMAT, Medical Faculty, [‡]DWI e.V. and Institute of Technical and Macromolecular Chemistry, [§]Department of Dermatology, Medical Faculty, and [⊥]Electron Microscopic Facility (EMF), Medical Faculty, RWTH Aachen, D-52074 Aachen, Germany, and [∥]Department of Materials Science and Engineering, Carnegie Mellon University, Pittsburgh, Pennsylvania 15213. [¶]These authors contributed equally to this work.

ABSTRACT Nanoparticle-based *in vivo* applications should consider the omnipresence of the phagocytes in the bloodstream and tissue. We have studied the nanoparticle uptake capacities of the most important human primary leukocyte populations using a nanoparticle library encompassing both rod-shaped and spherical gold nanoparticles with diameters between 15 and 50 nm and a variety of surface chemistries. Cetyltrimethylammoniumbromide (CTAB)-stabilized nanoparticles were internalized rapidly within 15 min and in large amounts by macrophages and to a lower extent also by monocytes. Interestingly, we found that the uptake of nanorods by macrophages was more efficient than that of nanospheres. Blocking experiments and electron microscopic studies revealed macropinocytosis as the major uptake mechanism. Grafting of poly(ethylene oxide) (PEO) onto the nanorods was found to significantly delay their internalization for several hours. The long-term uptake of PEO-coated nanoparticles with positively or negatively charged end groups was almost identical. Particle surface chemistry strongly influenced the expression of inflammation-related genes within 1 day. Furthermore, the macrophage phenotype was significantly affected after 7 days of culture with nanorods depending on the surface chemistry. Thus, *in vivo* application of nanoparticles with certain surface functionalities may lead to inflammation upon particle accumulation. However, our data also suggest that chemical modifications of nanoparticles may be useful for immunomodulation.

KEYWORDS: primary human blood phagocytes · gold nanorods · surface chemistry · cytokines · macropinocytosis

Gold nanoparticles (AuNPs) can be synthesized in various shapes and forms.[1] In addition to gold nanospheres (AuNSs), rod-shaped gold nanoparticles (AuNRs) have gained great interest due to their aspect-ratio-dependent additional absorption in the near-infrared spectrum that makes them suitable for *in vivo* hypothermal therapy.[2] In addition to shape, the surface chemistry of AuNPs can easily be modified. After preparation, colloidal AuNPs are usually stabilized by charged molecules such as citrate or cetyltrimethylammoniumbromide (CTAB), which may be exchanged by thiol functional compounds. Thus, the broadly accepted biocompatibility of gold nanoparticles together with the possibility to tailor both particle shape and surface chemistry predetermines them as a model system for cell interaction studies.

With the rise of nanotechnology and its applications in biomedicine, studies on the interaction of nanomaterials with cells have become increasingly important.[3] In the vast majority of cases, such studies are performed with cell lines. However, cell lines are immortal and might differ from primary cells in their nanoparticle uptake characteristics. HeLa cells (epithelial cells of cervical cancer) may be suitable to assess the general cytotoxicity of nanoparticles,[4] but caution is required when comparing particle uptake of HeLa cells to primary human cells, especially immune cells. Unlike primary human immune cells, the commonly used and non-human (particularly murine) macrophage cell lines show a high frequency of mutations and phenotypic and functional changes.[5] Furthermore, the human monocytic cell line THP-1 has a weak phagocytic capacity[6] in contrast to the strong phagocytic activity of monocytes or macrophages *in vivo* but also *in vitro*.[7]

The professional phagocytes are the most important cellular component of the innate immune system and are omnipresent in the body. They are represented by three types of immune cells: tissue macrophages, monocytes, and neutrophil granulocytes. The latter two circulate in the bloodstream where they encounter and remove bacteria and foreign particles.[7,8] In addition to the uptake capacities of monocytes, granulocytes encounter

*Address correspondence to mbartneck@ukaachen.de, groll@dwi.rwth-aachen.de.

Received for review February 8, 2010 and accepted May 21, 2010.

Published online May 27, 2010. 10.1021/nn100262h

nanoparticles by secretion of structures mainly composed of DNA that act as extracellular traps.[9] Human neutrophil granulocytes are 10 times more frequent in blood than monocytes. However, the latter may differentiate into the various subtypes of macrophages.[10] Among all phagocytes, macrophages are most efficient in internalization of body-foreign material or specially marked protein complexes, including bacteria, parasites, immunoglobulins, and also particles such as asbestos.[11] While most macrophages reside in tissue, the macrophages of the liver, the so-called Kupffer cells, are of special importance. They account for 80−90% of all macrophages of the body and are in direct contact with blood.[12] The well-documented underlying mechanisms of uptake are phagocytosis and macropinocytosis.[13,14] Actin filaments play an important role in all processes of internalization.[7]

As mentioned above, primary human blood phagocytes show comparable phagocytic activity *in vivo* and *in vitro*.[7] Hence, they are an ideal *in vitro* test platform for evaluation of the biological fate and consequences of nanoparticles in the human body. However, there are only limited data on the response of white blood cells to nanoparticles. The only internalization study with nanoparticles that focuses on primary human blood phagocytes used dextran-sedimented leukocytes, a mixture of granulocytes, lymphocytes, and monocytes.[15] Thus, differences between the three cell populations could not be determined, and the results comprise a combination of intracellular uptake of particles by monocytes and the extracellular trapping of neutrophils.[9] However, as concentration and overall presence of the subspecies in blood and in tissue vary strongly, a nanoparticle interaction study with better differentiation of leukocytes is necessary.

For long-term *in vitro* experiments, granulocytes cannot be used because they only have a half-life of about 1.5 days. In contrast, monocytes differentiate into long-living macrophages that are crucially involved in the induction of an inflammatory response. Particle uptake by macrophages may therefore trigger inflammation. From *in vivo* studies in mice, it is known that the continuous presence of nanoparticles in the body may induce inflammation in the liver.[16] A recent study using murine bone marrow macrophages has shown that gold nanoparticle peptide conjugates inhibit the proliferation and induce the expression of pro-inflammatory cytokines.[17] However, human mature macrophages do not proliferate and exhibit several functional differences compared to murine macrophages, for example, negligible expression of iNOS.[18]

Macrophages control the devolution of inflammation in the human body. There are two basic populations of macrophages which coexist *in vitro* and *in vivo*: pro-inflammatory macrophages (M1) that express the S100A8−S100A9 heterodimer that can be monitored using the 27E10 antibody,[19,20] and M2 (alternatively activated macrophages) among other antigens expressing the scavenger receptor CD163.[21] M1 may be activated by a pro-inflammatory stimulus or by signals from other immune cells. There are several different subclasses of M2 that down-regulate inflammation, promote angiogenesis, and are also involved in wound healing.[10]

In this study, we purified three different human leukocyte populations from human blood, granulocytes, lymphocytes, as well as monocytes and performed macrophage cell culture experiments to distinguish the levels of nanoparticle uptake. For the interaction studies, we have prepared a nanoparticle library that is based on AuNRs (15 × 50 nm) as well as AuNSs with 15 and 50 nm diameters, respectively. Stabilization of the nanoparticles was achieved by CTAB and thiol functional linear poly(ethylene oxide) (PEO) with either −OH, −COOH, or $-NH_2$ as end groups. Successful ligand exchange and stability of the nanoparticles were analyzed by transmission electron microscopy (TEM), ζ-potential measurements, and UV−vis spectroscopy. Thickness and grafting density of the PEO coatings was investigated by staining and TEM. Cells were incubated with the nanoparticles and checked for particle uptake both by seedless deposition and TEM. Beyond the quantification of particle uptake and the effect of shape and surface chemistry of the nanoparticles, we studied the effect of particle internalization on macrophage response on the level of gene expression, surface marker expression, and protein release.

RESULTS AND DISCUSSION

Nanoparticle Synthesis and Coating. AuNRs were synthesized by Ag(I)-assisted seeded growth and characterized by UV−vis and TEM analysis as published previously.[9,22,23] Exchange of CTAB with PEO was performed with commercially available 3 kDa α,ω-bifunctional PEOs that bear a thiol group at one end and either an alcohol, amino, or carboxy group at the other end of the polymer chain. UV−vis spectroscopy revealed that the aspect ratio of the nanorods was not affected by the coating procedure as recently reported.[9] For commercial gold nanospheres (AuNSs) with diameters of 15 and 50 nm, citrate was exchanged with CTAB for comparability with AuNRs. Table 1 presents ζ-potential measurements before and after polymer coating of the particles. Due to the positive charge of the CTA^+ ions, AuNR dispersions exhibit a strongly positive surface potential of about 90.0 mV. After ligand exchange and purification, the surface modification with linear HS−PEO−OH leads to ζ-potentials in the range of 0 to −5 mV for AuNRs and AuNSs. Because the method is not sensitive in the area around 0 mV (approximately 0 ± 10 mV), these values can be viewed as neutral. Carboxy-terminated PEO coating exhibits a negative (−20.2 mV) and the amine-terminated PEO a positive (+21.3 mV) ζ-potential. These results show that

TABLE 1. Zeta-Potential Measurements of the Nanoparticle Library at pH = 4 (w = peak width)[a]

	citrate	CTAB	HS−PEO_{3000}−OH	HS−PEO_{3000}−COOH	HS−PEO_{3000}−NH_2
15 nm AuNS	−39.3 mV (w = 8.9 mV)	+49.6 mV (w = 9.1 mV)	−4.5 mV (w = 3.5 mV)	−23.2 mV (w = 8.7 mV)	
15 × 50 nm AuNR		+90.0 m V (w = 9.4 mV)	−4.6 mV (w = 10.8 mV)	−20.2 mV (w = 5.3 mV)	+21.3 mV (w = 4.9 mV)
50 nm AuNS	−51.6 mV (w = 18.7 mV)	+59.0 mV (w = 9.2 mV)	6.5 mV (w = 6.3 mV)	−34.7 mV (w = 14.2 mV)	

[a]Partially published.[9]

PEO-stabilized AuNPs with hydroxyl, amine, or carboxy groups on the particle surface were obtained.

In addition to ζ-potential, the PEO coatings were visualized by TEM through staining with phosphotungstic acid (Figure 1). After staining of the purified PEO-stabilized AuNRs, a homogeneous layer with a dry width of 4 nm was obtained. Staining of CTAB-coated AuNRs did not result in contrast enhancement of the coating because the hydrophobic CTAB layer lacks interaction possibilities for the polar phosphotungstic acid. With a PEO layer thickness of 4 nm in the dry state, the grafting density of the linear PEO on the AuNRs can be calculated (for details, see Supporting Information). This yields a grafting density of 0.072, which corresponds to 0.8 chains/nm^2 and an average distance between neighboring chains (L) of 1.12 nm. In a good solvent, single polymer chains that are grafted to a solid surface with one end of the polymer chain occupy roughly a half-sphere with a radius comparable to the Flory radius for a random coil, R_F (3.77 nm for 3 kDa PEO; see Supporting Information).[24]

At grafting densities at which the surface area per chain, L^2, becomes smaller than R_F^2, individual chains start to overlap and the polymers begin to interact. This overlap criterion defines the so-called mushroom-to-brush transition in which the chains stretch out perpendicular to the surface. The attached polymer chains provide an effective steric barrier that stabilizes the particle against aggregation only in the brush regime. For our coatings, L^2 = 1.25 nm^2 is much smaller than R_F^2 = 14.21 nm^2, demonstrating that the coatings present a densely grafted layer in the brush regime. This high grafting density can be explained by the curvature of the nanoparticles that allows the PEO chains to occupy a cone-like volume segment in the coating in contrast to a cylinder-like volume segment for planar surfaces. As a result, the sterical restriction during the grafting process is lower and higher grafting densities can be reached more easily.

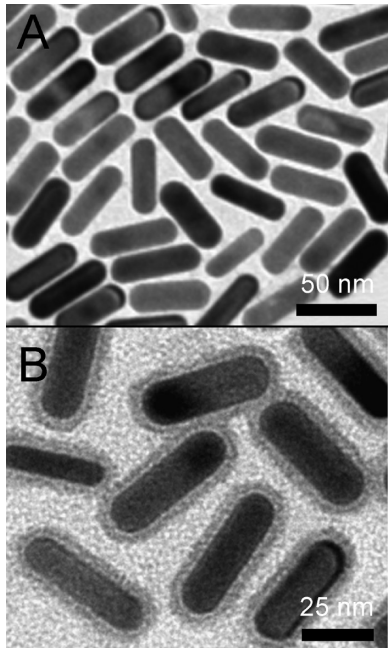

Figure 1. TEM images of CTAB-stabilized AuNRs after synthesis (A) and HS−PEO−COOH-coated AuNRs after phosphotungstic acid staining (B) as representative example for stained PEO coatings.

Stability of Nanoparticles in Human Serum and Cytotoxicity of Nanoparticles. The different nanoparticles were incubated in medium containing 5% human autologous serum at 1 OD for up to 7 days at 37 °C and afterward investigated using UV−vis spectroscopy and TEM. CTAB-stabilized particles immediately caused turbidity upon incubation with the medium and with time the formation of a precipitate, so that reliable UV−vis measurements were impossible and long-term incubations were not performed. This turbidity also occurred at lower particle concentrations. As the addition of CTAB to medium containing 5% serum also caused turbidity, this effect may be attributed to replacement of CTAB on the nanoparticle surface by serum proteins upon addition of the CTAB-stabilized nanoparticles to the serum and subsequent formation of aggregates mediated by free CTAB. In contrast, the dispersions of PEO-stabilized AuNPs stayed optically transparent over 7 days of incubation with serum and showed no significant change in maximum or shape of the absorption peak (Figure S1A, Supporting Information). TEM investigation showed that all PEO-modified nanoparticles remained individually dispersed without any indication of particle aggregation (Figure S1B). These results show that the PEO-stabilized particles are stable in medium containing serum and thus are suitable for long-term culture with cells.

Several studies have shown cytotoxic effects of the tenside CTAB on cell lines and, for example, on human nasopharyngeal carcinoma cells after 24 h.[25] In our studies, no cytotoxic effects of CTAB-coated AuNPs on primary human blood phagocytes were observed for at least 2 h of incubation (Figure S2). As phagocyte-mediated uptake typically takes place within 30 min, particle uptake studies were performed for up to 60

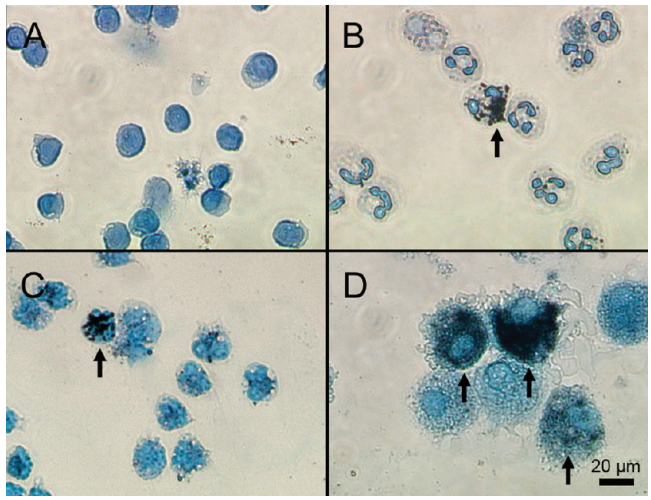

Figure 2. Cytospin preparations of (A) lymphocytes, (B) neutrophil granulocytes, (C) monocytes, and (D) macrophages after incubation with CTAB-coated AuNPs. Seedless deposition results in black spots or areas that indicate the presence of gold nanoparticles (highlighted by arrows).

min. Thus, an influence of cytotoxic effects on the results can be excluded. As expected, PEO-coated particles did not exhibit any cytotoxic effects even after incubation for 7 days.

To avoid cytotoxicity when cells were cultured with CTAB particles for 1 day or longer, cells were only incubated with the particles for 60 min. After this period of incubation with CTAB-coated particles, the cells had already internalized large amounts of particles (Figure 3). Thereafter, the medium containing the particles was replaced by fresh medium without nanoparticles. For PEO-coated particles, medium exchange was not performed. We found no negative effects of either CTAB- or PEO-coated particles on cell viability after 7 days of culture at 1 OD (>90% viable cells).

Uptake of CTAB-Stabilized AuNPs by Human Blood Phagocyte Populations. Seedless deposition of cytospin preparations has been used as a fast screening method for the detection of AuNP uptake by the cells. In this method, catalytic deposition of gold(I) ions occurs from solution onto the gold nanoparticles as metallic gold results in a continuous growth of the AuNP until an optically detectable black deposition is visible. As shown in Figure 2, black color indicates the presence of AuNPs, thus enabling the numerical determination of cells containing particles. We found that macrophages and monocytes internalized the CTAB-stabilized AuNPs, whereas lymphocytes did not. It should be noted that neutrophil granulocytes did not internalize the particles but trapped them in their extracellular structures (neutrophil extracellular traps) as we have reported recently.[9]

We have validated the seedless deposition protocol *via* TEM studies. As a representative example, Figure 3 presents a series of micrographs for the internalization of CTAB-coated AuNRs by monocytes. Figure 3A shows an image of a monocyte after incubation for 60 min. A closer look on the particle uptake process reveals that aggregates of particles attached to the cell surface (Figure 3B) with subsequent formation of protrusions around multiple particles (Figure 3C) followed by fusion with the membrane (Figure 3D) and vesicle formation (Figure 3E). The formations of particle aggregation as shown in Figure 3B were similarly observed for CTAB-coated gold spheres and may be attributed to interactions of the particles with serum components.

Figure 4 presents a more detailed study on the time- and concentration-dependent uptake of the CTAB-stabilized particles (15 × 50 nm AuNR, panels A−C; 15 nm AuNS, panels D−F; 50 nm AuNS, panels G−I) by the two blood phagocyte populations that actively internalized nanoparticles in our study, monocytes and macrophages. Panels A, D, and G show the amount of uptake-positive cells after 60 min of incubation with different particle concentrations. Statistical analysis showed that the concentration-dependent uptake of all kinds of particles follows a sigmoid dose−response curve with variable slope and $R^2 < 0.96$. Such sigmoid kinetics are a specific feature of the uptake of extracellular materials by mononuclear phagocytes.[26] For all particles, macrophages are more efficient in particle internalization than monocytes. To quantify these differences, we defined the concentration of particles at which more than 90% of the cells were positive for nanoparticle uptake as c_{Pmax} (on the basis of seedless deposition results). A detailed overview on uptake kinetics (c_{Pmax} and EC_{50}) is given in the Supporting Information (Table S1A,B). Moreover, monocytes show a clear effect of particle shape on uptake efficiency, with rod-shaped particles being taken up more efficiently than spheres. Interestingly, the smaller sized spheres with 15 nm diameter were taken up faster than the spheres with a diameter of 50 nm. The differences between macrophages and monocytes in particle uptake and the nanoparticle shape effect are clearer when the concentration dependence of particle internalization is evaluated in a time-dependent manner (Figure 4B,C,E,F,H,I). These panels show the uptake for low particle concentrations because at higher concentrations of particles no significant differences between both cell types were observed (data not shown). Especially at the lowest concentrations, macrophages were much more efficient in particle uptake than monocytes.

Three different parameters have to be considered to evaluate the impact on particle shape on the uptake rate: the different numbers of particles in the solutions at a certain optical density (OD), the concentration required for c_{Pmax}, as well as the different volumes of the particles. For a detailed calculation, see section 5 in the Supporting Information. Considering all parameters, the uptake of rods was about

230 times more efficient than that of spheres exhibiting the same diameter (15 nm) and 6-fold more efficient than the spheres of the same diameter as the length of the rods (50 nm). The morphological similarity of nanorods to protein capsules of virus particles may support their uptake.[27] Particularly, the rate of nanorod internalization may be of interest for applications in which these are administered in hyperthermal therapy.[2] It is noteworthy that the shape was found to be of minor importance for extracellular trapping by human immune cells.[9]

Quantification of Particle Uptake and Comparison to Other Cell Types and to Cell Lines. Recent research investigating the uptake of nanorods by cell lines required highly sensitive methods such as ICP-MS to detect the particles inside the cells.[28] For the particle uptake studies of primary human blood phagocytes, we chose a fast screening method which is based on cytospin preparations and seedless deposition that enables the investigation of the uptake of nanoparticles in a large number of cells. For comparison, we also examined the uptake of the CTAB-stabilized particles in HeLa cells and primary human fibroblasts under identical experimental conditions (Supporting Information Figure S3). Primary human fibroblasts, like lymphocytes, did not take up any particles. The difference of nanoparticle uptake between the phagocytes and HeLa cells is most obvious at low particle concentrations. At a particle density of as little as 0.8 OD, only 1% of the HeLa cells scored positive for particle uptake, while 90% of the monocytes and 95% of the macrophages showed internalized particles. Hence, the particle uptake by phagocytes was 80−100 times more pronounced than in HeLa cells, underlining both the efficient nanoparticle uptake by the phagocytes and the importance of a fast screening method.

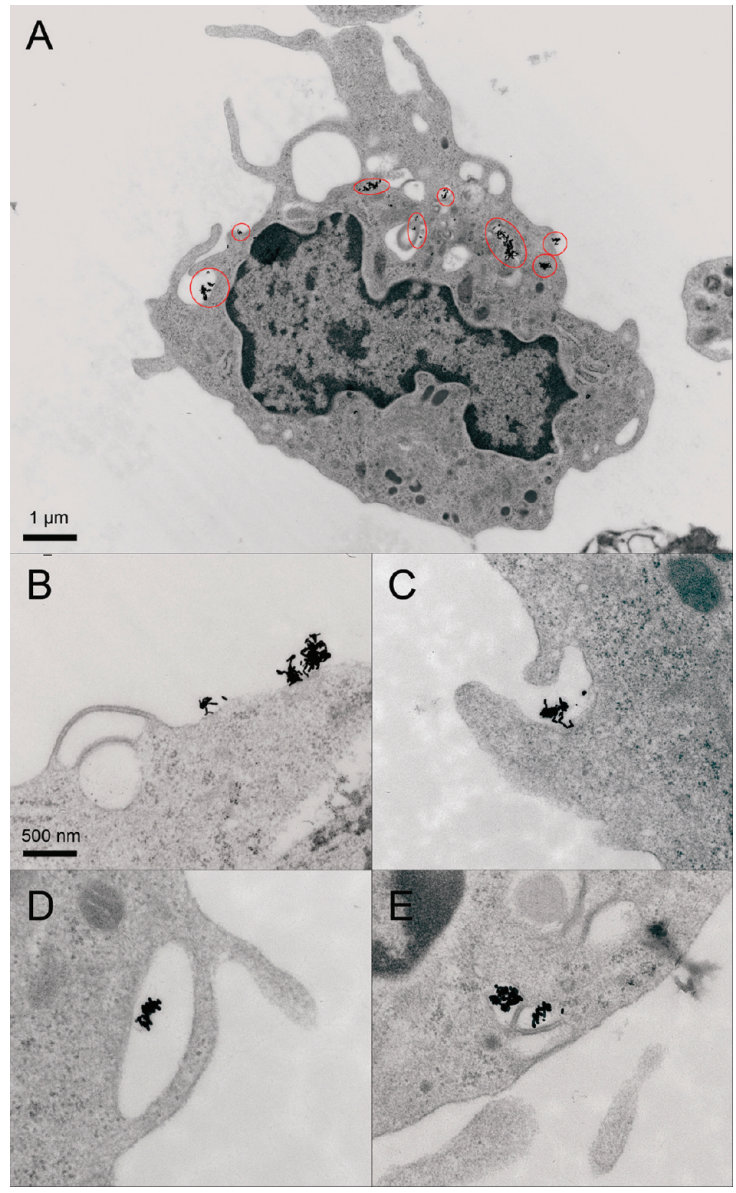

Figure 3. TEM studies of CTAB-coated AuNR uptake by primary human monocytes. (A) Monocyte after incubation with CTAB-stabilized AuNRs for 60 min at 1 OD. Red circles highlight AuNR presence. (B−E) Examples for different stages of AuNR uptake. The scale bar in panel B is representative for panels B−E.

To compare our data to published data about the uptake of CTAB-coated AuNRs by the cell line HT-29[28] and to determine the uptake capacities of human blood phagocytes, we approximated the number of CTAB-coated gold nanorods that were taken up by monocytes and macrophages after 60 min of incubation. As monocytes are smaller than macrophages (20 μm compared to 40 μm in diameter), they differ by a factor of 8 in cell volume, which was taken into account. In order to estimate the maximal efficiency of the uptake process, cells that showed strong particle uptake were chosen from ultrathin sections. A certain heterogeneity of the cell subpopulations might result in different particle uptake efficiency as, for example, $CD14^{high}$ $CD16^{+}$ monocytes exhibit an increased phagocytic activity compared to $CD14^{dim}$ $CD16^{+}$ monocytes.[29] On the basis of our TEM results, a single monocyte largely enriched with particles contained more than 80 000 rods; correspondingly, an enriched macrophage contained up to 1.3 million rods after 60 min of incubation with gold nanorods at 1 OD (see Supporting Information section 6 for details). For comparison with other cell types or cell lines, a recent study showed that a single HT-29 cell (a cancer cell line originating from colon carcinoma epithelium) was able to take up 46 CTAB-coated nanorods after 24 h.[28] This underlines that the uptake capacity of human primary blood phagocytes is significantly higher and occurs faster.

Inhibition of Nanoparticle Uptake by Phagocytes Using PEO Coating. Exchange of CTAB against PEO resulted in a significant inhibition of particle uptake within short-time

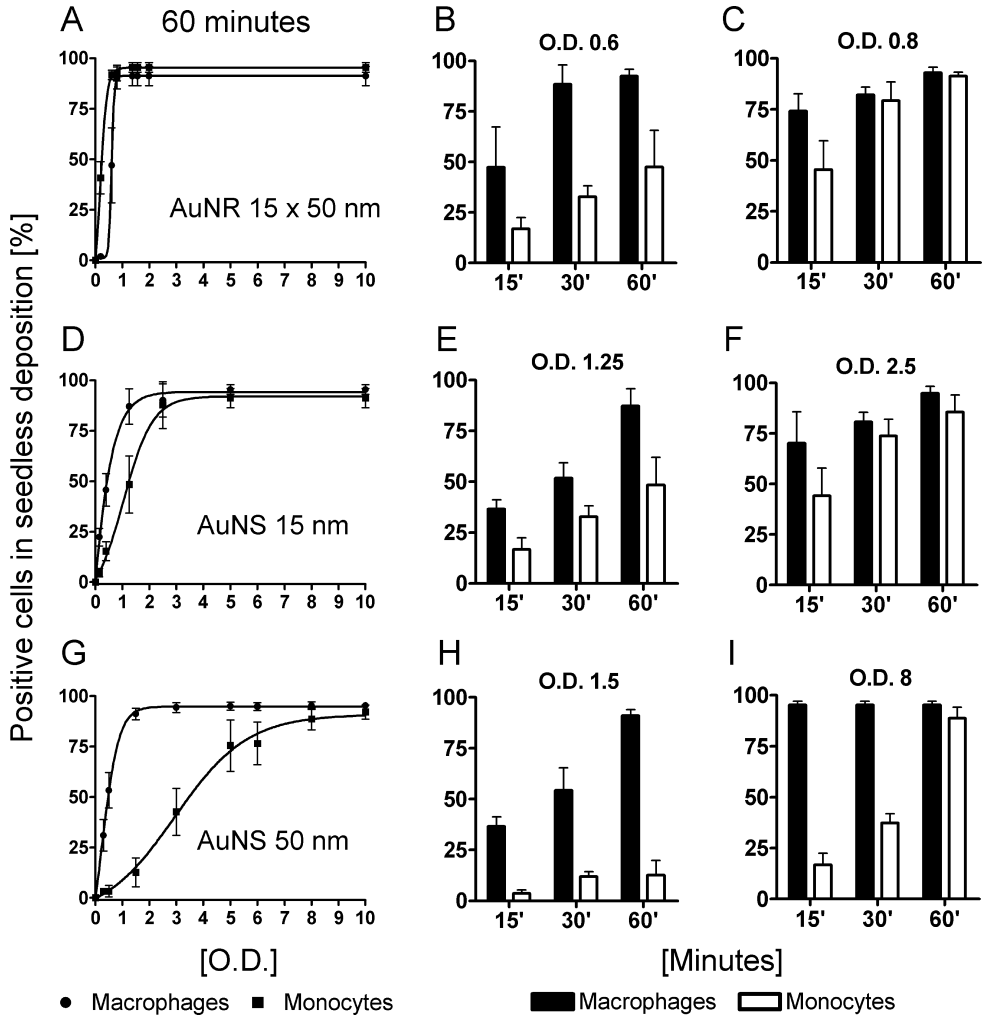

Figure 4. Concentration- and time-dependent uptake of CTAB-coated gold nanoparticles by human macrophages and monocytes as determined by seedless deposition. Data on the uptake after 60 min (A,D,G) were fit to a variable slope sigmoid equation. Time-dependent uptake of rods (A−C) as well as 15 nm (D−F) and 50 nm (G−I) spherules. Data represent mean values and standard deviation (n = 8).

incubation (Figure 5). Interestingly, the use of PEO with either COOH or NH_2 groups at the chain end that faces the surrounding solution did not lead to an increased uptake of these particles (similar to data obtained for the uptake of PEO−OH nanorods shown in Figure 5C), although the presence of ionic groups at the particle surface was expected to cause enhanced particle internalization. We explain these findings by a combined effect of surface curvature and graft molecular weight that reduces the exposure of polymer end groups to the environment.[30] Polymer chains grafted onto spherical surfaces occupy a cone-shaped volume segment of the coating, so that the volume available for each segment increases with growing distance from the particle surface. Thus, more relaxed chain conformations are expected for polymeric ligands when compared to flat surfaces where a grafted polymer chain occupies a cylindrical volume segment (see Supporting Information Figure S4). In agreement with this qualitative picture, self-consistent field simulations by Dan and Tirell as well as Wijmans and Zhulina have shown for constant length of surface-grafted chains the distribution of chain ends adopts more parabolic shape with increasing surface curvature (such as decreasing particle radius).[30,31] Thus, for small particles, surface interactions are expected to be independent of end group composition and are determined by the polymer backbone interaction. Our observations support this assertion (for details, see Supporting Information section 7).

To test whether PEO-stabilized nanorods are ingested by macrophages after longer incubation times, cells were incubated with these particles for 1 and 2 days. As shown in Figure 5C, cells showed uptake of PEO-coated rods after 24 h. Results were similar for amine- and carboxy-terminated PEO rods and spherules (data not shown). The number of macrophages with incorporated rods increased with time and concentration. It is interesting to note that the uptake of PEO rods did not reach the level of CTAB rod uptake even at the highest concentration of 5 OD and after 48 h (results were similar for PEO−NH_2 as well as for PEO−COOH rods). We found further that the PEO-

modified nanorods remained inside the cells even after 7 days of culture without changing their shape (Figure 5D,E).

It is known that coating of nanoparticles with PEO can prevent uptake by phagocytes within short time intervals.[15,32] Beyond that, we show in purified primary human blood phagocyte populations that despite the inhibition of the rapid uptake, which occurs already after 15 min (Figure 4), there also exists a time- and dose-dependent uptake for PEO-coated particles for up to 48 h of incubation (Figure 5C). This study shows the first kinetic data based on the uptake of PEO-coated nanoparticles in long-term cell culture with primary human blood phagocytes. These data might be of importance for improved understanding of the uptake of hydrogel nanoparticles by macrophages[33] and especially for PEO-coated gold nanorods that can used as a photocontrolled drug delivery system.[2,34]

Interestingly, the factors that are responsible for the intracellular uptake by immune cells are clearly different from extracellular trapping mechanisms. While particle uptake can be inhibited by PEO coating and no significant effect of functional end groups is observed (Figure 5C), we have recently shown that positive charges significantly enhance extracellular trapping of gold nanoparticles even if they were equipped with a PEO coating.[9]

Investigation of the Particle Uptake Mechanism Using Inhibitors of Phagocytosis. Macrophages express various receptors which are involved in the recognition of pathogens.[35] To further investigate molecular mechanisms of AuNP uptake by human immune cells, we inhibited typical uptake pathways which were described to be relevant for nanoparticles in a review article.[3] Gold nanoparticle uptake was almost completely suppressed at 4 °C (0.5% gold-including cells), demonstrating that the uptake is strongly energy-dependent.[36] Endocytosis can generally be inhibited using agents blocking the polymerization of actin, for example, cytochalasin D.[13] In our experiments, we found a dose-dependent inhibition of AuNP uptake at a maximum of 40 μM cytochalasin D; the number of cells containing gold was reduced to 29% (Figure 6). Higher concentrations of cytochalasin D resulted in decreased cell viability (data not shown). These results are similar to a study in which the uptake of 0.8 μm sized particles was partially inhibited by cytochalasin D treatment.[37] On the other hand, classical phagocytosis as for the uptake of *Toxoplasma* or *Candida* can be inhibited completely using as little as 10 μM of cytochalasin D,[38] indicating that nanoparticle internalization follows a mechanism different from classical phagocytosis.

The adsorption of serum proteins, in particular, immunoglobulins and complement factors, plays a major role in pathogen uptake.[39] The recognition of such molecules also called opsonins requires the respective receptors expressed by the cells. In the case of immunoglobulins, the Fc receptor[40] expressed by phagocytes can be inhibited using piceatannol.[41,42] Another important phagocytosis pathway is triggered by mannose receptors that recognize mannose and fucose, which are located on different pathogens[41] and which are also responsible for the transport of mannosylated nanoparticles.[35] The mannose receptor-mediated uptake can be blocked using high concentrations of mannan. We found that neither piceatannol nor mannan affected gold nanoparticle internalization (Figure 6). To exclude binding of complement protein present in serum, we also investigated the uptake in serum-free macrophage medium as well as in medium containing 5% fresh human serum as a source of complement protein. We found the uptake of the nanorods to be unaffected (not shown). To investigate the uptake of PEO−OH-coated rods as well, particles and cells were incubated in medium containing 5% human serum for 7 days before experiments were conducted. The uptake of these preincubated PEO-coated nanorods also occurred rapidly, similar to the rapid uptake of CTAB AuNRs that were used without preincubation.

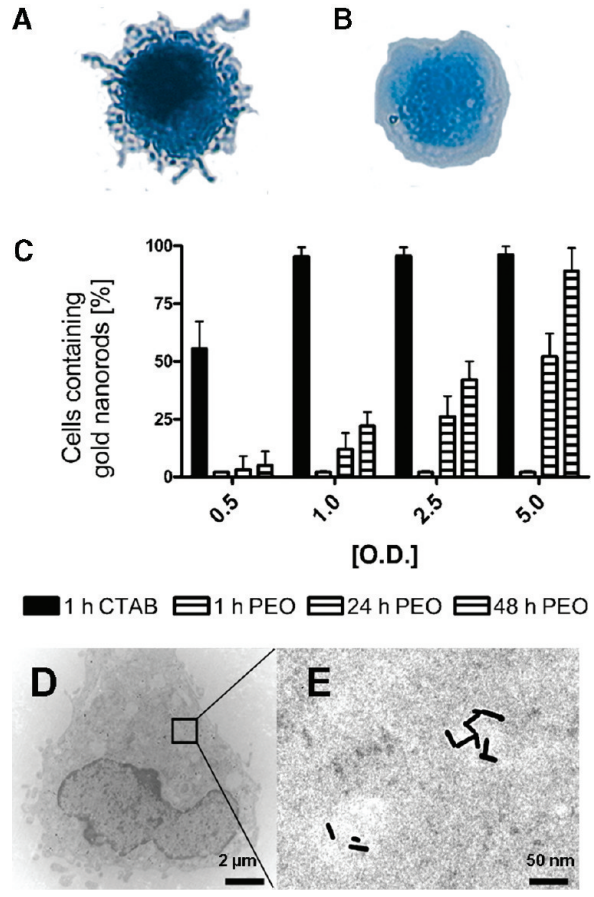

Figure 5. Macrophages after incubation with (A) CTAB- and (B) HS−PEO−OH-coated AuNRs for 60 min followed by seedless deposition. Black color indicates uptake of gold nanorods. (C) Time- and concentration-dependent uptake of CTAB- and PEO-coated nanorods. Data represent mean values and standard deviation ($n = 6$). (D,E) TEM of PEO-stabilized particles after 1 week culture with macrophages.

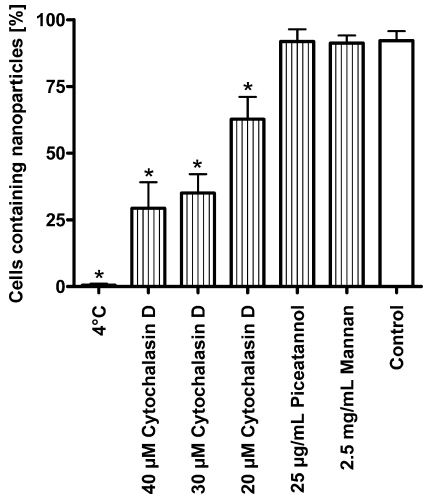

Figure 6. Inhibition of gold nanorod uptake by human macrophages using low temperature, cytochalasin D, piceatannol, and mannan after 60 min of incubation with CTAB-coated gold nanorods at 0.6 OD. Error bars represent standard deviation ($n = 6$); $P < 0.05$ indicates a significant difference compared to the untreated control.

The fact that serum-free medium does not reduce AuNR uptake and that heat inactivation of serum has no decreasing effect on AuNR uptake indicates that there is no unspecific binding of complement proteins or antibodies to nanorods that may increase their uptake as suggested previously.[3] Moreover, our findings show that the internalization of these nanoparticles is neither Fc-receptor-mediated, nor complement, nor mannose receptor-dependent as inhibitors on these pathways had no effect on particle uptake. In accordance with our TEM studies (Figure 3), the inhibitor studies suggest that the mechanism for the uptake of gold nanorods is macropinocytosis. This is supported by the size of the endocytosis vesicles (>1 μm).[13] Furthermore, the observed protrusions around the particles differed from the direct involution of the clathrin- or caveolin-mediated pinocytosis which lacks protrusions around particles and vesicles sizing of 60 or 120 nm.[13] Inhibitior studies also show that the mechanism is not a special type of receptor-mediated phagocytosis based on unspecific binding of antibodies, which would have been inhibited by piceatannol.[13,14,41]

It is known that protein adsorption or opsonization plays a crucial role for (nano)particle recognition and subsequent uptake by cells. Modification of particle surfaces with PEO is known to reduce protein adsorption and as common strategy to enhance circulation times in blood.[32] Gref and co-workers studied the effect of PEO polymer length and grafting density in self-assembled poly(lactic acid)−poly(ethylene oxide) copolymer nanoparticles on serum protein adsorption and particle uptake by blood phagocytes. They found that there is a threshold in PEO chain length in a molecular weight (M_w) range between 2000 and 5000, which results in a maximum reduction of serum protein adsorption, and that this threshold corresponds with minimization of short-term uptake by blood phagocytes.[15] They further showed that protein adsorption could not be completely prevented by coating with PEO and that albumin, fibrinogen, and apolipoproteins adsorb to PEO-coated particles. The calculated average polymer chain distance of surface-anchored PEO of 1.5 nm was the threshold for minimized protein adsorption and particle internalization by phagocytes. Similarly, a critical value of 0.5 chains/nm^2 (which corresponds to a PEO polymer chain distance of about 1.6 nm) has recently been identified as the threshold value for minimization of protein adsorption in self-assembled monolayers on flat gold substrates.[43]

Therefore, we hypothesize that the adsorption of serum proteins other than immunoglobulins and complement factors facilitates the uptake of the nanoparticles. In the case of CTAB-stabilized particles, serum protein adsorption is obviously due to turbidity of the solution upon incubation of the particles with serum and has been described before. The enhanced formation of particle aggregates results in rapid recognition and uptake by the phagocytes. For the PEO-stabilized particles, our experimentally determined average distance between surface-grafted PEO chains of 1.1 nm is well below the critical limit, and the stability of the particles in serum underlines the short-term prevention of protein adsorption. According to other studies, we thus attribute the inhibition of rapid uptake by the phagocytes to minimized protein adsorption. However, we could show that PEO-coated particles are also taken up with time, and that preincubation of the PEO-coated particles with serum for 7 days results in rapid uptake by the phagocytes. According to theoretical studies that show that PEO surfaces that efficiently prevent protein adsorption kinetically (meaning on short-term) may not be very efficient thermodynamically (meaning upon longer contact),[44] and we further hypothesize that slow but steady protein adsorption takes place also on the PEO-coated particles and this triggers recognition and uptake by the cells.

Effects of Nanoparticle Surface Chemistry on Inflammatory Gene Expression and Alteration of Phenotype. It has been shown that gold nanoparticles injected intravenously into mice were found in liver resident macrophages (Kupffer cells) but not in other tissues.[45] Furthermore, the conjugation of peptides to gold nanospheres induces an inflammatory response by murine macrophages.[17] In addition to the highly efficient uptake of nanoparticles by macrophages, attention should be drawn to the fact that monocytes circulating in the bloodstream also take up large amounts of particles (Figure 4 and Figure S3 in Supporting Information). After their migration into tissue, they differentiate into macrophages and there exists the possibility that the derived macrophages are preactivated due to the particles they internalized in blood. Such particles may, for example, be gold nanorods which were administered

intravenously in hyperthermal therapy.[2] To investigate the effects of nanoparticle surface chemistry on the differentiation of monocytes into macrophages and on the response of mature human primary macrophages, we first monitored the expression of selected macrophage genes: interleukin 1β (IL1β), IL8, IL10, myeloperoxidase (MPO), and Toll-like receptor 2 (TLR2). An LAL assay revealed that the nanoparticle solutions were free of bacterial products since the endotoxin content (LPS) was below the detection limit of the assay. Therefore, we exclude effects of bacterial components in nanoparticle solutions which would lead to an activation of macrophages.

As shown in Figure 7, the nanorods induced differential expression of important macrophage cytokines and a chemokine after 1 day of culture with macrophages (indicated by at least a 2-fold up or down-regulation of transcript level compared to the untreated control). The most strongly affected gene was IL8, thus it formed the first branch in clustering analysis. It was down-regulated 4-fold by PEO−OH- and down-regulated 20-fold by PEO−NH_2-coated rods. In contrast, CTAB- as well as PEO−COOH-coated rods led to up-regulation of IL8 (12-fold and 33-fold). The second branch included IL1β, which was both up-regulated by the PEO−OH- as well as the PEO−COOH-coated rods. CTAB-stabilized particles induced down-regulation of IL1β. The third branch included both MPO and IL10. MPO was down-regulated by PEO−OH- as well as PEO-NH_2-coated particles and up-regulated by the PEO−COOH and the CTAB coatings. IL10 was up-regulated by the particles coated with CTAB. TLR2, which was included in the fourth branch, was down-regulated by the amine as well as the hydroxy derivatives. Clustering analysis showed that MPO and IL10 were co-regulated by AuNRs. It further showed that the effects of AuNR coating with PEO−OH and PEO-NH_2 led to similar gene expression patterns reflected by the formation of one group. Coating with CTAB and PEO−COOH led to the formation of another group with different gene expression patterns (Figure 7).

IL8 is a pro-inflammatory chemokine with neutrophil-attracting activity.[46] Its differential expression in primary human macrophages induced by nanoparticle surface chemistry supports its consideration as an inflammatory marker in nanoparticle research. The pro-inflammatory cytokine IL1β is also strongly affected by surface chemistry. It is a central indicator for pro-inflammatory activation and control center of a protein network referred to as the inflammasome.[47] Our data also show that the abundance of the TLR2 transcript, which encodes a Toll-like receptor involved in pathogen recognition and in the activation of innate immunity, is not influenced by differences in surface chemistry. It is generally down-regulated by rod-shaped nanoparticles. We propose that this receptor may be involved in the uptake of nanoparticles because it was

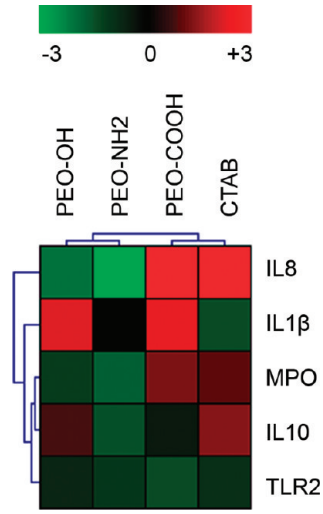

Figure 7. Change of gene expression in macrophages after 24 h of incubation with nanorods at 1 OD as measured using TaqMan-based real-time PCR. Clustering analysis showed that MPO and IL10 are co-regulated by nanorod surface chemistry and that the gene expression patterns of PEO−OH and PEO−NH_2 as well as PEO−COOH and CTAB are similar. Red color indicates up-regulation and green down-regulation of gene expression compared to the untreated control. Data represent mean values (n = 6).

shown that silver nanoparticles affect TLR signaling.[48] MPO codes for an enzyme that functions in the defense against pathogens, and more than two decades ago, it was shown to be involved in the response to foreign particles.[49] The regulation of IL10, a key suppressor of pro-inflammatory cytokines,[50] by nanoparticle chemistry is negligible.

Second, we also studied phenotypic alterations which are associated with distinct inflammatory functions. Flow cytometry analysis revealed that PEO−NH_2 coating significantly increased the number of anti-inflammatory (M2) macrophages expressing CD163 (Figure 8A) and decreased the number of pro-inflammatory macrophages (M1) which express 27E10 after 1 week of incubation (Figure 8B). PEO−COOH-stabilized rods induced the opposite effect (Figure 8A,B). The PEO−OH rods had no regulating effect on the expression of functional surface antigens. CD163 expressing macrophages appear in the down-regulatory phase of inflammatory processes. The antigen is also expressed by Kupffer cells and some other tissue resident macrophages.[21] Kupffer cells are known to show pronounced endocytic and phagocytic capacity.[51] In contrast, 27E10 positive macrophages are found in acute inflammatory tissues only.[19,20]

Amine termination of PEO did not induce the release of pro-inflammatory cytokines IL1β, IL6, TNFα, and CCL2 (Figure 8C−F). This is in accordance with the high number of cells expressing CD163 as revealed by flow cytometry since alternatively activated M2 inhibits inflammation and shows a decreased secretion of pro-inflammatory cytokines.[21] In contrast to the amine end

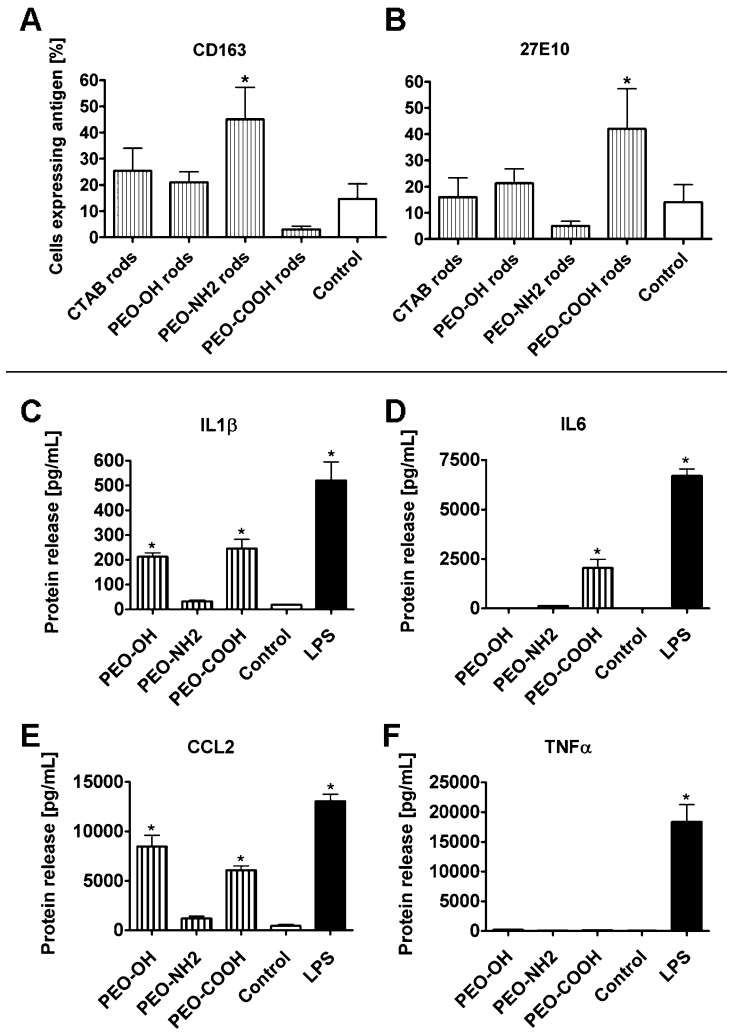

Figure 8. Expression of the macrophage surface antigens (A) CD163 (M2 subtype = anti-inflammatory) and (B) 27E10 (M1 phenotype = pro-inflammatory) after 7 days of culture with differently modified gold nanorods at 1 OD as determined using flow cytometry. Release of pro-inflammatory cytokines (C) IL1β, (D) IL6, (E) CCL2, and (F) TNFα. Bacterial lipopolysaccharide (LPS) was used as positive control for pro-inflammatory activation. Error bars represent standard deviation ($n = 6$); $P < 0.05$ indicates a significant difference compared to the untreated control.

groups, carboxy-modified nanoparticles enhanced the production of pro-inflammatory cytokines such as IL1β, IL6, and CCL2 (Figure 8C−F). PEO−OH-coated nanorods stimulated IL1β and CCL2 secretion but did not enhance IL6 and TNFα production (Figure 8C,E). Lipopolysaccharide (LPS) was used as positive control for pro-inflammatory activation.

In summary, these data show that the particles influence the expression of inflammatory-relevant genes and the phenotype of macrophages dependent on nanoparticle surface chemistry. Gold nanorods coated with PEO displaying amine end groups appear to exhibit anti-inflammatory properties, whereas carboxy end groups lead to pro-inflammatory effects. Neutrally charged PEO rods seem to exhibit only minor inflammatory effects in human macrophages.

The strong effect of the end group on macrophage response after long-term cell culture on macrophage response is an interesting observation since the uptake of nanoparticles is almost identical for neutral, positively, or negatively charged end groups on the PEO-coated nanoparticles. We explain this by the localization of the end groups within the PEO−polymer layer on the nanoparticle surface. As described above, before uptake into the cells, the end groups are only present at the nanoparticle surface to a minor extent. However, after particle internalization, the end groups may surface segregate with time and be exposed to the cell interior. This may be explained by interactions with proteins inside the cells especially *via* the end groups so that a driving force for surface segregation is generated. The nanorods may intracellularly act on specific inflammatory pathways since different proteins bind to either positively, neutrally, or negatively charged groups on the nanoparticle surface.

Applying our *in vitro* findings to the *in vivo* situation, we hypothesize that monocytes take up nanorods in the blood and later migrate into tissue where they differentiate into macrophages while still containing these particles; the resulting macrophages would exhibit strong changes in their inflammatory properties. Thus, our data indicate that rather simple chemical modifications of nanoparticle surfaces such as functionalization with amine groups may inhibit a pro-inflammatory reaction of phagocytic cells.

CONCLUSIONS

Our findings demonstrate that purified primary human blood phagocyte populations clearly show different potentials for the uptake of nanoparticles. In particular, macrophages and monocytes rapidly internalize nanoparticles with an efficiency and capacity that exceed unprofessional phagocytes such as HeLa cells by 2 orders of magnitude. Rod-shaped tenside stabilized particles are internalized with higher efficiency than tenside stabilized spheres with the same diameter as nanorod diameter in length. However, surface chemistry is dominant, and nanoparticle uptake can be inhibited for all particle geometries by surface modification using PEO irrespective of PEO end group functionality. However, this inhibition is limited to a period between 24 and 48 h depending on the particle concentration. Monocytes patrol the bloodstream, and the sinusoidal-lining macrophages in the liver and spleen also are in direct contact with the blood, opening a respective time window of up to 2 days for intravenously or intraperitoneally administered nanoparticles for targeted drug delivery applications.

Furthermore, the surface chemistry of gold nanorods has a strong effect on the activation state of human macrophages after particle internalization. Carboxy groups on the particle surface induce expression of mRNAs encoding pro-inflammatory proteins, while amino groups on the particle surface induce mRNAs encoding anti-inflammatory proteins. Hence, our data suggest that chemical modifications of nanoparticles may have immunomodulatory potency and that suitable coatings can open a time window for therapeutic application while at the same time preventing undesired pro-inflammatory effects.

In general, our results show clear differences in behavior between primary human cells and cell lines and emphasize the necessity of using primary human cells for studies on nanoparticle uptake. The fact that the uptake kinetics of human phagocytes are *identical in vitro* and *in vivo*[7] emphasizes the relevance of our results for the development of nanoparticle-based drug delivery systems.

EXPERIMENTAL METHODS

Nanoparticle Synthesis. Tetrachloroauric(III) acid monohydrate (≈52% Au), phosphotungstic acid, and CTAB were obtained from Fluka (Buchs, Switzerland). Silver nitrate, L-(+)-ascorbic acid, and sodium borohydride were purchased from Sigma-Aldrich (St. Louis, MO). PEO polymers (M_w 3000 Da) were obtained from Iris Biotech (Marktredwitz, Germany) and phosphate-buffered saline (PBS) without calcium or magnesium from Gibco (Grand Island, NY). If not stated otherwise, all reagents were used without further purification. For all nanoparticle syntheses, bidistilled water was used.

Nanorods were prepared *via* seed-mediated growth.[52] A growth solution was prepared by dissolving silver nitrate (0.01 mM), CTAB (0.08 M), and hydrogen tetrachloroauric(III) acid (0.42 mM) in bidistilled water followed by stirring at room temperature. The orange solution turned colorless upon addition of ascorbic acid (0.5 mM). A seed solution was prepared by dissolving CTAB (0.1 M) and hydrogen tetrachloroauric(III) acid (0.24 mM) in bidistilled water. Under vigorous stirring, freshly prepared, ice-cold aqueous sodium borohydride solution (0.6 mM) was added and the solution turned from orange to yellow-brown. The seed solution (12 μL) was added to the growth solution (10 mL) to start nanorod growth and was used 15 min after preparation. Nanorods were purified by two cycles of centrifugation (13 000 rcf, 20 min), removal of the supernatant and redispersion in PBS.

Citrate-stabilized spherical gold colloids were acquired from Aurion (Wageningen, The Netherlands) (d = 15 nm) and BBInternational (Cardiff, UK) (d = 50 nm). To coat 15 and 50 nm gold nanospheres with CTAB, spheres were diluted with bidistilled water to 0.7 OD. An excess of CTAB was added (0.13 M), and the solution was kept in an ultrasonic bath for 30 min at 60 °C and for 3.5 h at 40 °C. These CTAB-capped AuNSs were purified twice by centrifugation at 13 000 rcf for 15 min without cooling and redissolved in one-third of their original volume.

Ligand Exchange. PEO modification of all nanoparticles with either OH, COOH, or NH_2 as end groups was performed by a ligand exchange protocol for the coating of CTAB-capped gold nanorods (AuNRs) with alkanethiols.[53] The purified nanoparticles were diluted in bidistilled water (1:5), 1 mL of 2.5 mM ethanolic PEO solution was added, and the solution was sonicated as explained above. Afterward, CTAB was removed by extraction with chloroform followed by centrifugation (11 000 rcf, 10 min). The concentrated nanoparticle dispersion was diluted with 0.9 wt % isotonic NaCl solution or PBS buffer to the desired concentration.

Nanoparticle Characterization. Ligand exchange and stability of the nanoparticles as well as the dispersions in human serum were analyzed with transmission electron microscopy (TEM) using a Zeiss Libra 120 TEM (Zeiss, Oberkochen, Germany) at 120 kV, ζ-potential measurements using a Zetasizer Nano Z from Malvern Instruments (Worcestershire, UK), and UV−vis spectroscopy using a UV160A from Shimadzu (Tokyo, Japan).

Staining of purified nanorod samples was performed using 7 mM phosphotungstic acid solution in water. Thirty microliters of nanorod solution was put on a TEM grid coated with Formvar and carbon. After 30 s, the droplet was removed, and to the wet grid was added 9 μL of the staining solution. After another 30 s, the droplet was removed again and the sample was dried at room temperature.

Concentration of Nanoparticles and Endotoxin Testing. To determine particle concentration, the absorption (here also called optical density, OD) of dilute dispersions of nanospheres was measured at the respective absorption peak for 15 and 50 nm AuNSs diluted in bidistilled water. In the case of nanorods, the optical density of the solution at the maximum of the longitudinal plasmon resonance peak ($\lambda_{max,long}$ at approximately 850 nm) in bidistilled water was used. To compare concentrations of spherical and rod-shaped nanoparticles at a specific OD, the particle concentration of AuNRs and AuNSs was estimated.[22,23] Briefly, absorption cross sections were calculated to be $C_{abs} = 6.9 \times 10^{-15}$ m^2 for nanorods (for $\lambda_{max,long}$ at 850 nm), $C_{abs} = 6.0 \times 10^{-17}$ m^2 for 15 and $C_{abs} = 3.0 \times 10^{-15}$ m^2 for 50 nm nanospheres. In order to compare particle numbers in solution, these values were used to determine particle concentrations at 1 OD according to Lambert−Beer's law ($c_{AuNR} = 1.45 \times 10^7$/μL, $c_{AuNS,15\ nm} = 1.67 \times 10^9$/μL, $c_{AuNS,50\ nm} = 3.33 \times 10^7$/μL). A limulus amebocyte lysate (LAL) assay QCL-1000 was obtained from Lonza (Walkersville, MD) to test endotoxin of nanoparticles solutions. The kit was used according to the instructions of the manufacturer.

Isolation and Culture of Human Primary Immune Cells. Cells and serum were isolated from healthy volunteers (the local Ethics commission gave ethical approval for this study, and informed consent was obtained from all participants). To obtain serum from venous whole blood samples, blood was clotted for 1 h at 37 °C, centrifuged three times at 3000 rcf, and heat inactivated for 60 min at 57 °C. To generate fresh serum as a source for complement proteins, heat inactivation was omitted. Heterologous serum was prepared by pooling serum from at least three donors. Before using, serum was filtered (0.2 μm). To isolate granulocytes from heparinized venous whole blood, erythrocyte sedimentation was performed by incubation for 30 min at 37 °C in 1% dextran in PBS. The leukocyte containing phase was used for Ficoll-Paque (Amersham Pharmacia Biotech, Freiburg, Germany) density gradient centrifugation for further separation of granulocytes. To isolate peripheral blood mononuclear cells (PBMC), density gradient centrifugation was carried out, as well. Monocytes were isolated from PBMC using the Dynal Monocyte Negative Isolation Kit (Invitrogen, Carlsbad, CA) according to the manufacturer instructions. Lymphocytes were isolated by incubation of PBMC at 37 °C on Petri dishes at a density of three million cells/mL in RPMI1640 containing 5% human autologous serum for 35 min. During this period, monocytes become adherent and lymphocytes were removed with the supernatant. To obtain monocyte-derived macrophages (MDM), monocytes were cultured for 7 days in sterile (3.2 cm) bacterial grade Petri dishes (Becton Dickinson, Franklin Lakes, NJ) at a density of one million cells/mL in RPMI1640 medium obtained from Sigma-Aldrich (St. Louis, MO) supplemented with 5% autologous serum in a humidified 5% CO_2 incubator. Macrophages were harvested using a silicon cell scraper (Roth, Karlsruhe, Germany). All methods for cell isolation resulted in a purity of at least 95% as estimated by Giemsa staining of cytospin preparations. Cell viability was assessed using Trypan Blue staining. Bacterial lipopolysaccharide (LPS) was obtained from Sigma-Aldrich (St. Louis, MO) and was

used to stimulate macrophages for 24 h at day 6 of culture at a concentration of 1 μg/mL.

Seedless Deposition. For short-term incubation for up to 3 h, cells and AuNPs were incubated in RPMI1640 with 5% serum under continuous shaking conditions (500 rpm) at 37 °C in 1.5 mL tubes on a Thermomixer comfort (Eppendorf, Hamburg, Germany). All long-term experiments (>24 h) were performed under cell culture conditions as described above. Nanorod dispersions were added so that the final concentration was 1 OD. Prior to long-term incubation with CTAB-coated particles, monocytes were incubated for 2 h with the particles. During this incubation, the monocytes remained attached to the plastic and internalized large amounts of CTAB-coated nanoparticles. The medium containing free CTAB that is potentially toxic under long-term conditions[28] was removed and replaced with medium containing 5% serum. Following the incubation, nanoparticles were removed from cell suspensions by washing three times with PBS. Cytospin preparations were made using a Cytospin II centrifuge (Shandon, Runcorn, England). Cytospins were fixed with 2% paraformaldehyde in PBS for 5 min. To visualize internalized gold for light microscopy, the GoldEnhance LM Kit 2112 (Nanoprobes, Yaphank, NY) was used according to the instructions of the manufacturer. Thiazine staining was performed to counterstain cells blue. Duplicates from each preparation were evaluated by counting 200 cells for calculation of uptake percentages. Gray and black discolored cells were considered as positive. Negative controls were performed to control background signals.

Transmission Electron Microscopy. To prepare cells for transmission electron microscopy, cells were washed three times with PBS after their incubation with AuNPs. Subsequently, the cells were fixed in 3% glutaraldehyde (in 0.1 M Soerensen's phosphate buffer, pH 7.4; 13 mM $NaH_2PO_4 \times H_2O$; 87 mM $Na_2HPO_4 \times 2H_2O$) for 22 h. Fixed cells were washed with 0.1 M Soerensen's phosphate buffer overnight, embedded in 2% agarose, followed by 1 h incubation in 1% OsO_4 (in 17% sucrose buffer with pH 7.4; 88 mL of 0.1 M Soerensen's phosphate buffer; 12 mL of distilled water, and 17 g of sucrose), rinsed with distilled water and dehydrated with ethanol (30−100%) and propylenoxide (100%). Cell processing was performed by embedding in Epon, polymerization for 8 h at 37 °C and 56 h at 60 °C. Finally, preparations were cut into 70−100 nm thick slices and contrasted with uranyl acetate and lead citrate. The samples were analyzed with an EM 400 T (Philips, Amsterdam, The Netherlands) at 60 kV, and micrographs were taken by a CCD camera MORADA (Olympus, Tokyo, Japan).

Inhibitors. Cytochalasin D was purchased from Sigma Aldrich (St. Louis, MO) and resolved in dimethyl sulfoxide (DMSO). Piceatannol was obtained from A.G. Scientific (San Diego, CA) and used at 25 μg/mL concentration after resolving in DMSO. Bacterial D-mannose (mannan) was purchased from Fluka (Buchs, Switzerland), and 2.5 μg/mL was used in the experiments. Macrophage serum-free medium was obtained from Gibco (Carlsbad, CA). Incubation of cells at 4 °C was performed on a Thermomixer comfort (Eppendorf, Hamburg, Germany) under serum conditions. In all blocking experiments, cells were incubated for 30 min with the inhibitors before adding the particles.

Real-Time PCR. RNA was isolated using the High Pure RNA isolation kit (Roche, Basel, Switzerland). Reverse transcription of 500 ng of RNA was performed using the High Capacity RNA to cDNA kit (Applied Biosystems, CA) according to the instructions of the manufacturer. Universal PCR master mix and TaqMan gene expression assays (Applied Biosystems, CA) probes (CD163, IL1β, IL10, CXCL8, S100A9, and MPO) were used for the highly specific detection of cDNA in a total volume of 25 μL per experiment using a 7300 real-time PCR system (Applied Biosystems, CA). Data were collected at stage 3, step 2 (60.0 @ 1:00) in the standard 7300 run mode. We tested three different house keeping genes (β-actin, tubulin, and glyceraldehyde 3-phosphate dehydrogenase) and found that β-actin was least affected of all house keeping genes by nanoparticles. CT values were generated automatically and related to the endogenous control gene β-actin. Untreated macrophages were used as reference for the calculation of gene expression.

Hierarchical Clustering Analysis and Gene Expression Heat Maps. To prepare data for HCA, reciprocals were calculated for all expression values between 0 and 1. Positive values indicate up-regulation of the gene and negative ones indicate down-regulation. HCA was performed using average linkage as agglomeration rule and with Euclidean distance. In the heat map, the brightest red squares represent up-regulation and the green color indicates down-regulation. Black squares indicate that there was neither up- nor down-regulation in comparison to the control. On the basis of the similarity of the gene expression values in HCA, genes and the experiments were assigned to groups separately if they were similar or form their own branch. The benefit of HCA is to identify similar gene expression patterns of the different nanorods as well as the co-regulation of genes. Gene expression was considered up- or down-regulated if the $\log_2$ values between the reference and the sample were higher than 1 (greater than 2-fold increase) or lower than 1 (greater than 2-fold decrease), respectively. The heat map was generated using the Genesis Software Package.[54]

Flow Cytometry. Cell surface antigens were double-stained with the phycoerythrin (PE)-conjugated monoclonal antibody CD163 (clone GHI/61) (R&D Systems, Minneapolis, MN) and the fluorescein isothiocyanate (FITC)-conjugated 27E10 antibody (BMA Biomedicals AG, Augst, Switzerland) according to the instructions of the manufacturer. Flow cytometry analysis was performed using a FACSCalibur and the BD CellQuest Pro software version 5.2.1 (Becton Dickinson, Franklin Lakes, NJ). All results are given relative to the untreated control.

Cytokine Detection. The release of 14 different cytokines (CCL2, CCL3, CCL4, CSF-3, CXCL8, CXCL9, CXCL10, IFNγ, IL1β, IL6, IL10, IL12p70, TNFα, and TNFβ) into the culture medium was measured using the FlowCytomix system in collaboration with the producing company (Bender Medsystems, Vienna, Austria). The system of cytokine detection is based on antibody-coupled microbead populations of which each specifically binds a certain cytokine. Measurements were performed in duplicates at 50 μL sample volume. The overall intra-assay variation of the system was less than 10%. All results on differential cytokine release are based on the comparison to the untreated control.

Statistical Analysis. Statistical analysis of the biological data was performed using Graph Pad Prism 4.0 (GraphPad Software, La Jolla, CA). One- or two-way ANOVA with Bonferronis post test was performed to test significance of uptake data. $P < 0.05$ was considered as statistically significant. Nonlinear regression of data was performed using the sigmoid dose−response function with variable slope.

Acknowledgment. This work was supported by the DFG research training group "Biointerface" (GRK1035), the BMBF (13N9176 "Nano-SRT"), the EU (FP 6) as well as the Interdisciplinary Centre for Clinical Research (IZKF "BioMAT") within the faculty of medicine at the RWTH Aachen. Human dermal fibroblasts were kindly provided by Yvonne Marquardt, Department of Dermatology, Medical Faculty, RWTH Aachen. We thank Bender Medsystems for assistance with cytokine measurement, and Rebecca Ludvigsen for the proofreading of the manuscript.

Supporting Information Available: Additional results on the stability of the nanoparticles, calculations on the enhanced uptake of nanorods compared to nanospheres and on the comparison of gold nanorod uptake by professional and unprofessional phagocytes. This material is available free of charge *via* the Internet at http://pubs.acs.org.

REFERENCES AND NOTES

1. Grzelczak, M.; Perez-Juste, J.; Mulvaney, P.; Liz-Marzan, L. M. Shape Control in Gold Nanoparticle Synthesis. *Chem. Soc. Rev.* **2008**, *37*, 1783–1791.
2. Oyelere, A. K.; Chen, P. C.; Huang, X.; El-Sayed, I. H.; El-Sayed, M. A. Peptide-Conjugated Gold Nanorods for Nuclear Targeting. *Bioconjugate Chem.* **2007**, *18*, 1490–1497.
3. Dobrovolskaia, M. A.; McNeil, S. E. Immunological Properties of Engineered Nanomaterials. *Nat. Nanotechnol.* **2007**, *2*, 469–478.

4. Pan, Y.; Neuss, S.; Leifert, A.; Fischler, M.; Wen, F.; Simon, U.; Schmid, G.; Brandau, W.; Jahnen-Dechent, W. Size-Dependent Cytotoxicity of Gold Nanoparticles. *Small* **2007**, *3*, 1941–1949.
5. Chamberlain, L. M.; Godek, M. L.; Gonzalez-Juarrero, M.; Grainger, D. W. Phenotypic Non-equivalence of Murine (Monocyte-) Macrophage Cells in Biomaterial and Inflammatory Models. *J. Biomed. Mater. Res. A* **2009**, *88*, 858–871.
6. Bazile, D.; Prud'homme, C.; Bassoullet, M. T.; Marlard, M.; Spenlehauer, G.; Veillard, M. Stealth Me.PEG-PLA Nanoparticles Avoid Uptake by the Mononuclear Phagocytes System. *J. Pharm. Sci.* **1995**, *84*, 493–498.
7. Schwarzer, E.; De Matteis, F.; Giribaldi, G.; Ulliers, D.; Valente, E.; Arese, P. Hemozoin Stability and Dormant Induction of Heme Oxygenase in Hemozoin-Fed Human Monocytes. *Mol. Biochem. Parasitol.* **1999**, *100*, 61–72.
8. Mollinedo, F.; Borregaard, N.; Boxer, L. A. Novel Trends in Neutrophil Structure, Function and Development. *Immunol. Today* **1999**, *20*, 535–537.
9. Bartneck, M.; Keul, H. A.; Zwadlo-Klarwasser, G.; Groll, J. Phagocytosis Independent Extracellular Nanoparticle Clearance by Human Immune Cells. *Nano Lett.* **2010**, *10*, 59–63.
10. Martinez, F. O.; Sica, A.; Mantovani, A.; Locati, M. Macrophage Activation and Polarization. *Front. Biosci.* **2008**, *13*, 453–461.
11. Suzuki, Y. Interaction of Asbestos with Alveolar Cells. *Environ. Health Perspect.* **1974**, *9*, 241–252.
12. Bilzer, M.; Roggel, F.; Gerbes, A. L. Role of Kupffer Cells in Host Defense and Liver Disease. *Liver Int.* **2006**, *26*, 1175–1186.
13. Conner, S. D.; Schmid, S. L. Regulated Portals of Entry into the Cell. *Nature* **2003**, *422*, 37–44.
14. Aderem, A.; Underhill, D. M. Mechanisms of Phagocytosis in Macrophages. *Annu. Rev. Immunol.* **1999**, *17*, 593–623.
15. Gref, R.; Luck, M.; Quellec, P.; Marchand, M.; Dellacherie, E.; Harnisch, S.; Blunk, T.; Muller, R. H. 'Stealth' Corona-Core Nanoparticles Surface Modified by Polyethylene Glycol (PEG): Influences of the Corona (PEG Chain Length and Surface Density) and of the Core Composition on Phagocytic Uptake and Plasma Protein Adsorption. *Colloids Surf. B* **2000**, *18*, 301–313.
16. Cho, W. S.; Cho, M.; Jeong, J.; Choi, M.; Cho, H. Y.; Han, B. S.; Kim, S. H.; Kim, H. O.; Lim, Y. T.; Chung, B. H.; Jeong, J. Acute Toxicity and Pharmacokinetics of 13 nm-Sized PEG-Coated Gold Nanoparticles. *Toxicol. Appl. Pharmacol.* **2009**, *23*, 16–24.
17. Bastus, N. G.; Sanchez-Tillo, E.; Pujals, S.; Farrera, C.; Kogan, M. J.; Giralt, E.; Celada, A.; Lloberas, J.; Puntes, V. Peptides Conjugated to Gold Nanoparticles Induce Macrophage Activation. *Mol. Immunol.* **2009**, *46*, 743–748.
18. Weinberg, J. B.; Misukonis, M. A.; Shami, P. J.; Mason, S. N.; Sauls, D. L.; Dittman, W. A.; Wood, E. R.; Smith, G. K.; McDonald, B.; Bachus, K. E.; *et al.* Human Mononuclear Phagocyte Inducible Nitric Oxide Synthase (iNOS): Analysis of iNOS mRNA, iNOS Protein, Biopterin, and Nitric Oxide Production by Blood Monocytes and Peritoneal Macrophages. *Blood* **1995**, *86*, 1184–1195.
19. Zwadlo, G.; Voegeli, R.; Osthoff, K. S.; Sorg, C. A Monoclonal Antibody to a Novel Differentiation Antigen on Human Macrophages Associated with the Down-Regulatory Phase of the Inflammatory Process. *Exp. Cell Biol.* **1987**, *55*, 295–304.
20. Odink, K.; Cerletti, N.; Bruggen, J.; Clerc, R. G.; Tarcsay, L.; Zwadlo, G.; Gerhards, G.; Schlegel, R.; Sorg, C. Two Calcium-Binding Proteins in Infiltrate Macrophages of Rheumatoid Arthritis. *Nature* **1987**, *330*, 80–82.
21. Zwadlo, G.; Voegeli, R.; Osthoff, K. S.; Sorg, C. A Monoclonal Antibody to a Novel Differentiation Antigen on Human Macrophages Associated with the Down-Regulatory Phase of the Inflammatory Process. *Exp. Cell Biol.* **1987**, *55*, 295–304.
22. Keul, H. A.; Moeller, M.; Bockstaller, M. R. Shape-Evolution of Gold Nanorods under Controlled Secondary Growth Conditions. *Langmuir* **2007**, *23*, 10307–10315.
23. Keul, H. A.; Moeller, M.; Bockstaller, M. R. Effect of Solvent Isotopic Replacement on the Structure Evolution of Gold Nanorods. *J. Phys. Chem. C* **2007**, *112*, 13483–13487.
24. De Gennes, P.-G. Conformations of Polymers Attached to an Interface. *Macromolecules* **1980**, *13*, 1069–1075.
25. Leonov, A. P.; Zheng, J.; Clogston, J. D.; Stern, S. T.; Patri, A. K.; Wei, A. Detoxification of Gold Nanorods by Treatment with Polystyrenesulfonate. *ACS Nano* **2008**, *2*, 2481–2488.
26. Thilo, L.; Stroud, E.; Haylett, T. Maturation of Early Endosomes and Vesicular Traffic to Lysosomes in Relation to Membrane Recycling. *J. Cell. Sci.* **1995**, *108*, 1791–803.
27. Kovacs, F. A.; Denny, J. K.; Song, Z.; Quine, J. R.; Cross, T. A. Helix Tilt of the M2 Transmembrane Peptide from Influenza A Virus: An Intrinsic Property. *J. Mol. Biol.* **2000**, *295*, 117–125.
28. Alkilany, A. M.; Nagaria, P. K.; Hexel, C. R.; Shaw, T. J.; Murphy, C. J.; Wyatt, M. D. Cellular Uptake and Cytotoxicity of Gold Nanorods: Molecular Origin of Cytotoxicity and Surface Effects. *Small* **2009**, *5*, 701–708.
29. Skrzeczynska-Moncznik, J.; Bzowska, M.; Loseke, S.; Grage-Griebenow, E.; Zembala, M.; Pryjma, J. Peripheral Blood $CD14^{High}$ $CD16^{+}$ Monocytes Are Main Producers of IL-10. *Scand. J. Immunol.* **2008**, *67*, 152–159.
30. Dan, N.; Tirrell, M. Polymers Tethered to Curved Interfaces. A Self-Consistent-Field Analysis. *Macromolecules* **1992**, *25*, 2890–2895.
31. Wijmans, C. M.; Zhulina, E. B. Polymer Brushes at Curved Surfaces. *Macromolecules* **1993**, *26*, 7214–7224.
32. Gref, R.; Minamitake, Y.; Peracchia, M. T.; Trubetskoy, V.; Torchilin, V.; Langer, R. Biodegradable Long-Circulating Polymeric Nanospheres. *Science* **1994**, *263*, 1600–1603.
33. Hamidi, M.; Azadi, A.; Rafiei, P. Hydrogel Nanoparticles in Drug Delivery. *Adv. Drug Delivery Rev.* **2008**, *60*, 1638–1649.
34. Niidome, T.; Yamagata, M.; Okamoto, Y.; Akiyama, Y.; Takahashi, H.; Kawano, T.; Katayama, Y.; Niidome, Y. PEG-Modified Gold Nanorods with a Stealth Character for *In Vivo* Applications. *J. Controlled Release* **2006**, *114*, 343–347.
35. Taylor, P. R.; Martinez-Pomares, L.; Stacey, M.; Lin, H. H.; Brown, G. D.; Gordon, S. Macrophage Receptors and Immune Recognition. *Annu. Rev. Immunol.* **2005**, *23*, 901–944.
36. Kuiper, J. W.; Pluk, H.; Oerlemans, F.; van Leeuwen, F. N.; de Lange, F.; Fransen, J.; Wieringa, B. Creatine Kinase-Mediated ATP Supply Fuels Actin-Based Events in Phagocytosis. *PLoS Biol* **2008**, *6*, e51.
37. Tse, S. M.; Furuya, W.; Gold, E.; Schreiber, A. D.; Sandvig, K.; Inman, R. D.; Grinstein, S. Differential Role of Actin, Clathrin, and Dynamin in Fc Gamma Receptor-Mediated Endocytosis and Phagocytosis. *J. Biol. Chem.* **2003**, *278*, 3331–3338.
38. Ryning, F. W.; Remington, J. S. Effect of Cytochalasin D on *Toxoplasma gondii* Cell Entry. *Infect. Immun.* **1978**, *20*, 739–743.
39. Bredt, W.; Kist, M.; Jacobs, E. Phagocytosis and Complement Action. *Isr. J. Med. Sci.* **1981**, *17*, 637–640.
40. Wernersson, S.; Karlsson, M. C.; Dahlstrom, J.; Mattsson, R.; Verbeek, J. S.; Heyman, B. IgG-Mediated Enhancement of Antibody Responses Is Low in Fc Receptor Gamma Chain-Deficient Mice and Increased in Fc Gamma RII-Deficient Mice. *J. Immunol.* **1999**, *163*, 618–622.
41. Araki, N.; Hatae, T.; Furukawa, A.; Swanson, J. A. Phosphoinositide-3-Kinase-Independent Contractile Activities Associated with FcGamma-Receptor-Mediated Phagocytosis and Macropinocytosis in Macrophages. *J. Cell. Sci.* **2003**, *116*, 247–257.
42. Ezekowitz, R. A.; Gordon, S. Interaction and Regulation of Macrophage Receptors. *Ciba Found. Symp.* **1986**, *118*, 127–136.
43. Unsworth, L. D.; Sheardown, H.; Brash, J. L. A Random Sequential Adsorption Model for Protein Adsorption to

Surfaces Functionalized with Poly(ethylene oxide). *Langmuir* **2008**, *24*, 1924–1929.
44. Satulovsky, J.; Carignano, M. A.; I.; Szleifer, I. Kinetic and Thermodynamic Control of Protein Adsorption. *Proc. Natl. Acad. Sci. U.S.A.* **2000**, *97*, 9037–9041.
45. Sadauskas, E.; Wallin, H.; Stoltenberg, M.; Vogel, U.; Doering, P.; Larsen, A.; Danscher, G. Kupffer Cells are Central in the Removal of Nanoparticles from the Organism. *Part Fibre Toxicol.* **2007**, *4*, 10.
46. Van Damme, J.; Rampart, M.; Conings, R.; Decock, B.; Van Osselaer, N.; Willems, J.; Billiau, A. The Neutrophil-Activating Proteins Interleukin 8 and Beta-Thromboglobulin: *In Vitro* and *In Vivo* Comparison of NH2-Terminally Processed Forms. *Eur. J. Immunol.* **1990**, *20*, 2113–2118.
47. Martinon, F.; Burns, K.; Tschopp, J. The Inflammasome: A Molecular Platform Triggering Activation of Inflammatory Caspases and Processing of ProIL-Beta. *Mol. Cell* **2002**, *10*, 417–426.
48. Castillo, P. M.; Herrera, J. L.; Fernandez-Montesinos, R.; Caro, C.; Zaderenko, A. P.; Mejias, J. A.; Pozo, D. Tiopronin Monolayer-Protected Silver Nanoparticles Modulate IL-6 Secretion Mediated by Toll-like Receptor Ligands. *Nanomedicine* **2008**, *3*, 627–635.
49. Shepherd, V. L. The Role of the Respiratory Burst of Phagocytes in Host Defense. *Semin. Respir. Infect.* **1986**, *1*, 99–106.
50. Bogdan, C.; Vodovotz, Y.; Nathan, C. Macrophage Deactivation by Interleukin 10. *J. Exp. Med.* **1991**, *174*, 1549–1555.
51. Kmiec, Z. Cooperation of Liver Cells in Health and Disease. *Adv. Anat. Embryol. Cell Biol.* **2001**, *161*, 1–151.
52. Nikoobakht, B.; El-Sayed, M. A. Preparation and Growth Mechanism of Gold Nanorods (NRs) Using Seed-Mediated Growth Method. *Chem. Mater.* **2003**, *15*, 1957–1962.
53. Yu, C.; Nakshatri, H.; Irudayaraj, J. Identity Profiling of Cell Surface Marers by Multiplex Gold Nanorod Probes. *Nano Lett.* **2007**, *7*, 2300–2306.
54. Sturn, A.; Quackenbush, J.; Trajanoski, Z. Genesis: Cluster Analysis of Microarray Data. *Bioinformatics* **2002**, *18*, 207–208.